Topology Synthesis of Compliant Mechanisms for Nonlinear Force-Deflection and Curved Path Specifications

A. Saxena

G. K. Ananthasuresh

Department of Mechanical Engineering and Applied Mechanics, University of Pennsylvania, Philadelphia, PA 19104-6315

Optimal design methods that use continuum mechanics models are capable of generating suitable topology, shape, and dimensions of compliant mechanisms for desired specifications. Synthesis procedures that use linear elastic finite element models are not quantitatively accurate for large displacement situations. Also, design specifications involving nonlinear force-deflection characteristics and generation of a curved path for the output port cannot be realized with linear models. In this paper, the synthesis of compliant mechanisms is performed using geometrically nonlinear finite element models that appropriately account for large displacements. Frame elements are chosen because of ease of implementation of the general approach and their ability to capture bending deformations. A method for nonlinear design sensitivity analysis is described. Examples are included to illustrate the usefulness of the synthesis method. [DOI: 10.1115/1.1333096]

Introduction

Compliant mechanisms transmit motion and force by virtue of the elastic deformation of their flexible members. When flexural joints (notches or living hinges) are used in compliant mechanisms to connect segments that are relatively more rigid, the motion is restricted to a small range. If the motion is large, the stresses in a flexural hinge exceed the material strength causing failure. Distributed compliant segments help increase the range of motion by distributing the stresses more or less evenly throughout the device. While this is advantageous from the viewpoint of functionality and performance, it makes the design procedure more difficult as we must now account for the nonlinearity associated with large displacements, rotations, and sometimes strains. With the kinematics based approach [1,2], such mechanisms can be synthesized for path generation and force-deflection specifications using the *pseudo rigid body models*. These models accurately represent the nonlinear behavior in large deformation of uniform beams with end loads. This technique is suitable if the topology (i.e., the type of mechanism as in a four-bar, a six-bar, etc.) is known *a priori*. Alternatively, the continuum mechanics based technique [3–6] offers a synthesis procedure for generating the optimal topology, shape, and size of compliant mechanisms for prescribed specifications.

The design intent in the continuum mechanics based approach thus far has been to determine an optimal topology based on the conflicting objectives of maximizing both the flexibility and stiffness of a compliant continuum. Ananthasuresh et al. [3] used the deformation at the prescribed output port and strain energy as respective measures of flexibility and stiffness, and proposed a multi-criteria formulation wherein the weighted linear combination of the two objectives was optimized. Frecker et al. [4] and Nishiwaki et al. [7] posed the multi-criteria objective as maximizing the ratio of the output deformation and strain energy to improve the convergence behavior in optimization. Saxena and Ananthasuresh [8] proposed an energy based formulation wherein the available output energy which is proportional to the square of the output displacement was used as a measure for flexibility. This was maximized while the input energy which is proportional to the input displacement was minimized. The flexibility and stiffness measures in the multi-criteria formulations were generalized by Saxena and Ananthasuresh [9] and a structural property was derived using the first order necessary conditions for an optimum. The property states that *the ratio of the mutual strain energy density and strain energy density is uniform throughout the compliant continuum*. A similar formulation was stated by Sigmund [5] wherein the mechanical advantage of the mechanism was maximized with constraints on volume and input displacements. Larsen et al. [10] presented the synthesis of compliant topologies with multiple input and output ports. Hetrick and Kota [11] employed size and shape optimization techniques to improve compliant topologies by maximizing the mechanical efficiency subject to the desired mechanical or geometric advantage requirements.

In all the aforementioned, linear finite element models were employed in the synthesis procedure. Linear elastic analysis based optimization generates solutions that are accurate only qualitatively. That is, the resulting solution will have the output port move in a specified direction for a given input force, or maximum ratio of output displacement or force to input displacement or force instantaneously at the beginning of motion. Since linear models are not accurate for large ranges of motion, prescribed specifications cannot be met exactly in the quantitative sense. Recently, Bruns and Tortorelli [12] and Buhl et al. [13] used nonlinear finite element analysis in topology generation of mainly structures along with few examples of compliant mechanisms using density based plane stress elements to attain desired deflection at the output port for single input loads. In this paper, we present methods for topology generation of compliant mechanisms with prescribed nonlinear output deflection characteristics for multiple loads. A work concurrent to this is by Pedersen et al. [14] who have employed geometrically nonlinear plane stress models for topology optimization of large deflection compliant mechanisms.

To account for large elastic deformations of flexible members in compliant mechanisms, incorporation of nonlinear finite element procedures is essential in topology synthesis algorithms. Such an approach makes possible to model large deformation accurately when designing compliant mechanisms (Fig. 1(*a*)). Using nonlinear continuum models, compliant mechanisms can be synthesized requiring the output port to satisfy prescribed nonlinear force-deflection specifications (Fig. 1(*b*)). The output port can also be required to trace a prescribed curved path (Fig. 1(*c*)) for a

Contributed by the Mechanisms Committee for publication in the JOURNAL OF MECHANICAL DESIGN. Manuscript received Sept. 1999. Associate Editor: C. M. Gosselin.

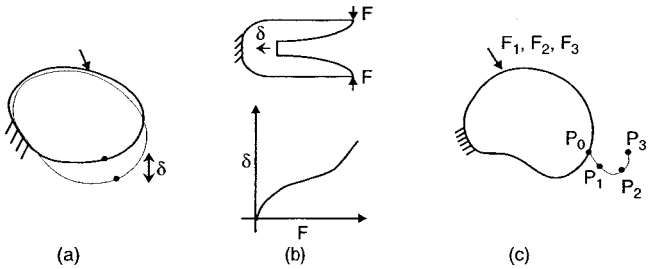

Fig. 1 Synthesis capabilities using nonlinear finite element analysis (*a*) quantitative accuracy for large deformations (*b*) prescribed nonlinear force-deflection specifications (*c*) curved output paths

given set of input loads. Synthesizing compliant topologies with aforementioned design requirements is not possible using linear continuum models due to the inherent assumption of the continuum stiffness being invariant with the design and/or large displacements. In this paper, the concept of geometric nonlinearity and its relevance in design for prescribed nonlinear deflection characteristics is first explained using a simple one dimensional bar example. Finite element equations for frame elements are later used in this work to represent the geometrically nonlinear continua. Frame elements are capable of capturing bending modes and are easy to implement with the topology generation schemes. Direct differentiation and adjoint variable methods are discussed and employed to compute design sensitivities analytically. Several examples are included to illustrate the design procedures for compliant mechanisms using existing flexibility-stiffness multi-criteria synthesis formulations, and with prescribed force-deflection specifications and curved output paths.

Elastic Analysis with Geometric Nonlinearity

Two kinds of nonlinearities, namely *material* and *geometric* can occur in a deforming structure when the applied loads are large. Material nonlinearity refers to the nonlinear relationship between the stresses and strains in a continuum and so depends on the constitutive properties of the material. Geometric nonlinearity, on the other hand, results due to *large displacements* or *rotations*. As an example, consider a bar (Fig. 2) pivoted at one end and guided along a vertical straight line at the other end. Although very simple, it illustrates the essential features of geometric nonlinearity and is therefore often used in literature [15,16]. This example is used in this paper to present the implementation details of analytical displacement sensitivities later.

With the second order terms retained in the strain, the force-deflection relationship, $F_{ext}(y)$ can be obtained as

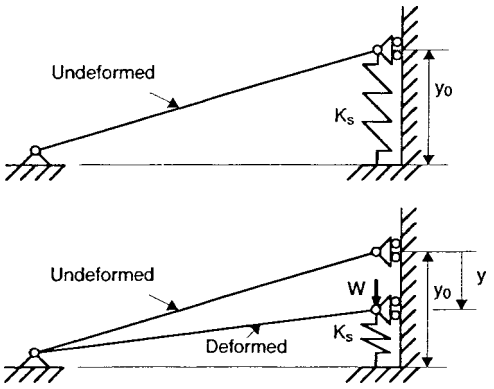

Fig. 2 A bar with geometrically nonlinear deformation

$$F_{ext} \equiv F_{int} = W = \frac{EA}{l^3}\left(y_o^2 y - \frac{3}{2} y_o y^2 + \frac{1}{2} y^3\right) + K_s y \tag{1}$$

with

$$g = W - F_{ext} = W - \frac{EA}{l^3}\left(y_o^2 y - \frac{3}{2} y_o y^2 + \frac{1}{2} y^3\right) - K_s y \tag{2}$$

where

E = Young's Modulus of the material
A = cross-section area of the bar
y_o = initial (undeformed) position of the bar
K_s = spring constant of the linear spring attached to the roller end
l = undeformed length of the bar
F_{int} = internal force in the bar resisting the output load, F_{ext}
g = force residual

The internal force, F_{int} on the right hand side of Eq. (1) can be differentiated with respect to y to obtain the tangent stiffness constant, K_t, which plays the same role as the stiffness matrix used in the finite element analysis. That is,

$$K_t = \frac{dg}{dy} = \frac{dW}{dy} = \frac{EA}{l^3}\left(y_o^2 - 3y_o y + \frac{3}{2} y^2\right) + K_s \tag{3}$$

which can be rearranged as

$$K_t = \left\{\frac{EA}{l}\left(\frac{y_o}{l}\right)^2 + K_s\right\} + \left\{\frac{EA}{l}\left(\frac{y^2 - 2y_o y}{l^2}\right)\right\} + \left\{\frac{N}{l}\right\} \tag{4}$$

where, N is the axial force in the bar given by

$$N = EA\left\{\frac{1}{2}\left(\frac{y}{l}\right)^2 - \frac{y y_o}{l^2}\right\} \tag{5}$$

Note that the stiffness, K_t of the bar now depends on the design, EA/l^3, the initial displacement, y_0 and the spring, K_s at the roller end, as opposed to being a constant. In Eq. (4), the first term is the linear stiffness effect while the second and third terms are due to *large-displacement* and *initial stress* respectively. The initial stress term arises due to the axial force, N that accumulates in the bar as it continues to deform under increasing load, W. Figure 3(*a*) compares the linear and nonlinear force-deflection characteristics and Fig. 3(*b*) shows the tangent stiffness matrix and its linear and nonlinear constituents.

The tangent stiffness constant, K_t is used to solve Eq. (1) numerically with small increments in W as shown below.

$$K_t \Delta y = \Delta W \tag{6}$$

The net deflection, y can be accumulated from each increment as

$$\Delta y_k = \frac{\Delta W_k}{(K_t)_k} \tag{7}$$

$$y_{k+1} = y_k + \Delta y_k \tag{8}$$

Alternatively, Eq. (1) can be solved iteratively by applying W all at once. It is more efficient to combine the incremental and iterative methods as explained next for the general case.

Numerical Procedures for Geometrically Nonlinear Analysis

In a general case with multi degrees of freedom, the equilibrium equations in the nonlinear finite element setup can be written as

$$\mathbf{g} \equiv \mathbf{F}_{int}(\mathbf{x_o} + \mathbf{p}) - \mathbf{F}_{ext} = \mathbf{0} \tag{9}$$

where $\mathbf{g}$ is the force residual; $\mathbf{F}_{int}(\mathbf{x_o} + \mathbf{p})$ are the internal forces at respective degrees of freedom expressed in a fixed (global) reference frame and depend on the initial global configuration, $\mathbf{x}_o$; and

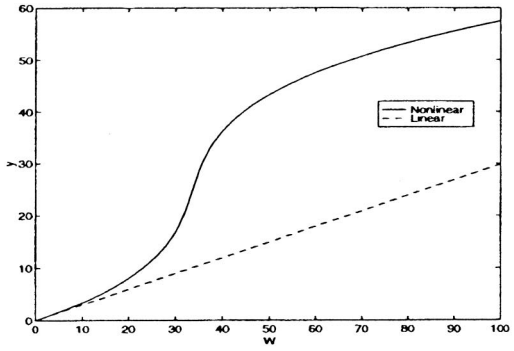

(a)

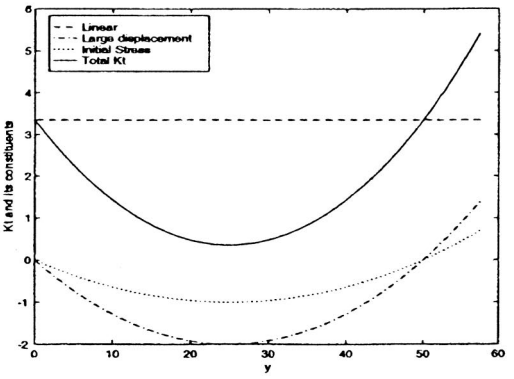

(b)

Fig. 3 (*a*) **Linear and nonlinear force-deflection relationship for the one-dimensional bar in Fig. 2** (*b*) **tangent stiffness matrix,** K_t **and its constituents** ($E=2\times10^5$ **N/mm**^{2}, $A=250$ **mm**^{2}, $y_o=25$ **mm**, $I=2500$ **mm**, $K_s=1.35$ **N/mm**)

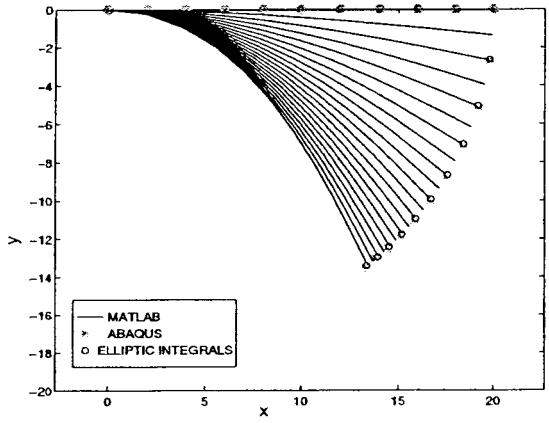

(a)

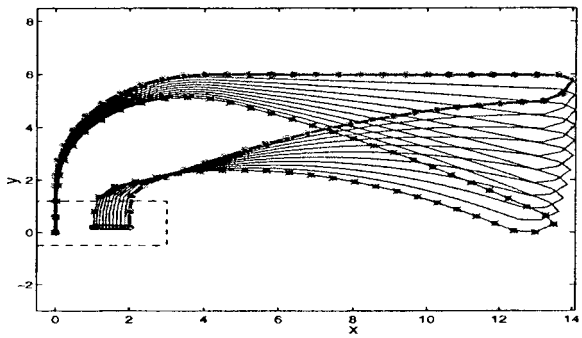

(b)

Fig. 4 (*a*) **Geometrically nonlinear analysis of a cantilever beam in Matlab for a vertical end force of** -20 **N.** (*b*) **Comparison of the output port deformation for a symmetric half of the deformed compliant crimper.**

the net displacements, $\mathbf{p}$; and $\mathbf{F}_{ext}$ are the respective applied loads. The internal force vector can be computed using the principle of virtual work. Rewriting the equations using the first order Taylor series expansion about an equilibrium position, $(\mathbf{x}_o+\mathbf{p})$, yields

$$\mathbf{F}_{int}(\mathbf{x_o}+\mathbf{p})+\mathbf{K}_t(\mathbf{x_o}+\mathbf{p})\Delta\mathbf{p}=\mathbf{F}_{ext}+\Delta\mathbf{F}_{ext} \tag{10}$$

with

$$\mathbf{K}_t(\mathbf{x}_o+\mathbf{p})=\frac{\partial\mathbf{g}}{\partial\mathbf{p}}=\frac{\partial\mathbf{F}_{int}}{\partial\mathbf{p}}$$

where the differential displacements, $\Delta\mathbf{p}$ are due to the incremental external load vector, $\Delta\mathbf{F}_{ext}$ and $\mathbf{K}_t$ is the tangent stiffness matrix. Combining Eqs. (9) and (10) results in

$$\mathbf{K}_t(\mathbf{x}_o+\mathbf{p})\Delta\mathbf{p}=\Delta\mathbf{F}_{ext} \tag{11}$$

Equilibrium equations can be solved using *incremental, iterative* or a combination of the two approaches [15,16]. The incremental approach requires that the external loads be applied in small load increments. The procedure is well suited for problems where it is desired to trace the entire equilibrium path. However, the accuracy in the incremental approach is adversely affected if the load increments are large. The *iterative* approach on the other hand uses the Newton-Raphson's iterative technique to obtain the displacements for a given external load. In each iteration, the residual, $\mathbf{g}$ in Eq. (9) computed as the difference between the external and internal force vectors is forced to zero by suitably computing the differential displacements. It is generally preferred to combine the two solution procedures to trace the equilibrium path accurately for large external loads.

Frame finite elements with shallow arch Kirchhoff's beam theory are employed in this paper to represent large displacement nonlinear continua. The finite element formulation to obtain the internal force vector and tangent stiffness matrix is well archived in the literature [15,16]. The quasi-Eulerian approach [15] is used with combined incremental-iterative approach wherein the nodal coordinates, $\mathbf{x}_o$ are held fixed during the iterative procedure and incremental displacements, $\Delta\mathbf{p}$ are obtained to satisfy equilibrium equations for a given load increment. Thereafter, nodal coordinates are updated using the transformation, $\mathbf{x}=\mathbf{x}_o+\Delta\mathbf{p}$ for the subsequent load increment and the displacements are set to zero. The updated configuration is treated as reference $(\mathbf{x}_o=\mathbf{x})$ and the procedure is repeated. In this work, Green strain measure is used during the iterative procedure while Almansi strain measure is employed in the incremental updates. The geometrically nonlinear analysis is implemented in Matlab™ [17] and compared with the elliptic integral based analytical solutions and commercially available finite element software ABAQUS™ [18]. Figure 4(*a*) shows the deformation results of a cantilever beam modeled using 10 frame elements each with cross-sectional area and moments of inertia of 5 mm^2 and $1.95\times$mm^4 respectively, and the Young's modulus of 100 GPa. Results are obtained for a downward vertical load of 20 N applied at the tip in 20 increments. The maximum error incurred when compared with both elliptic integral solutions and ABAQUS using B21 beam elements is 2.3%. The performance of the code is also compared using the compliant crimper example. The symmetric half of the crimper with the load and displacement boundary conditions solved in Matlab™ [17] is shown in Fig. 4(*b*). With the same geometry and material speci-

fications of the elements as in the previous example, a vertically downward load of 20 N is applied at the input port. The error in the two solution procedures is less than 1%.

Sensitivity Analysis

To apply optimization algorithms, sensitivities of displacement based objectives with respect to the design variables are needed. Using the finite difference method to compute these sensitivities can be computationally expensive. This is because the number of nonlinear finite element analyses required is equal to the number of elements in the discretized continuum assuming that a design variable is associated with each element. Therefore, an efficient and accurate method to compute the sensitivities is sought. Either the *adjoint variable method* or the *direct differentiation method* [19] can be employed to compute the design sensitivities analytically. With the adjoint variable method, a linear adjoint equation [20–22] is obtained for each constraint and explicit expressions are obtained in terms of design velocity fields. On the other hand, the direct differentiation method involves obtaining the first variation of the state with respect to the design. This is accomplished by solving the linear equations resulting from the differentiation of the original nonlinear equilibrium equations with respect to the design variables. Both methods yield the same accuracy in design sensitivity information and that the difficulties involved in the numerical implementation are equivalent [19].

Computing analytical displacement sensitivities is first explained using the one dimensional example described earlier followed by the extension to the general case with multi degrees of freedom. Differentiating Eq. (2) at equilibrium ($g=0$) with respect to the cross section area A, we get

$$\frac{dg}{dA}=\frac{\partial g}{\partial A}+\frac{\partial g}{\partial y}\frac{dy}{dA}=0 \tag{12}$$

Rearranging Eq. (12) gives

$$\frac{dy}{dA}=-\left[\frac{\partial g}{\partial y}\right]^{-1}\frac{\partial g}{\partial A} \tag{13}$$

Since the external force, F_{ext} is a constant, $\partial g/\partial A=\partial F_{int}/\partial A$ and also $\partial g/\partial y$ can be identified as the tangent stiffness constant, K_t. Then, from Eq. (13) we have

$$\frac{dy}{dA}=-K_t^{-1}\frac{\partial F_{int}}{\partial A} \tag{14}$$

or

$$\frac{dy}{dA}=-\frac{E(y_o^2y-\frac{3}{2}y_oy^2+\frac{1}{2}y^3)}{EA(y_o^2-3y_oy+\frac{3}{2}y^2)+l^3K_s} \tag{15}$$

Eq. (15) can be verified by analytically differentiating Eq. (1), setting it to zero and solving for dy/dA. When the sensitivity cannot be obtained symbolically as in Eq. (15), which is the case in general, it is computed incrementally as below.

$$\frac{dy}{dA}=-K_t^{-1}\sum_{j=1}^{N_{inc}}\left(\frac{\partial\Delta F_{int}}{\partial A}\right)_j \tag{16}$$

where N_{inc} is the total number of increments and ΔF_{int} is the internal force within each increment, j. It should be noted that $(\partial F_{int}/\partial A)$ is accumulated in each increment.

The general case, which is presented next, uses the approach shown in Eq. (16). Two methods called the *direct differentiation* and *adjoint variable* exist for the sensitivity analysis which are discussed next.

Direct Differentiation Method

Rewriting equilibrium Eqs. (9) as a function of the m-dimensional design variable vector, $\mathbf{b}$, we have

$$\mathbf{g}(\mathbf{b},\mathbf{p})\equiv\mathbf{F}_{int}(\mathbf{b},\mathbf{p})-\mathbf{F}_{ext}=\mathbf{0} \tag{17}$$

where $\mathbf{F}_{int}$ and $\mathbf{F}_{ext}$ are the internal and external loads respectively, and $\mathbf{p}$ are the net displacements computed using the quasi-Eulerian approach. Note that internal forces are implicit functions of the updated configuration, $\mathbf{x}$. To compute the design sensitivity of a function $\psi(\mathbf{b},\ \mathbf{p})$, where $\psi(\mathbf{b},\ \mathbf{p})$ generically represents the objective and constraints, differentiated with respect to the design variable vector to yield

$$\frac{d\psi(\mathbf{b},\mathbf{p})}{d\mathbf{b}}=\frac{\partial(\mathbf{b},\mathbf{p}^c)}{\partial\mathbf{b}}+\frac{\partial\psi(\mathbf{b}^c,\mathbf{p})}{\partial\mathbf{p}}\frac{d\mathbf{p}}{d\mathbf{b}} \tag{18}$$

where the superscript, c implies that the variable is held constant during partial differentiation. Eq. (18) involves the ordinary derivatives of the state variables, $\mathbf{p}$ with respect to the design, $\mathbf{b}$ which can be computed using state Eq. (17). This constitutes a major computation in the sensitivity analysis. Differentiating Eqs. (17) with respect to the design yields

$$\left[\frac{\partial\mathbf{g}}{\partial\mathbf{p}}\right]\left(\frac{d\mathbf{p}}{d\mathbf{b}}\right)=-\frac{\partial\mathbf{g}}{\partial\mathbf{b}} \tag{19}$$

Since $\mathbf{F}_{ext}$ is constant in the absence of body forces, we have

$$\frac{\partial\mathbf{g}}{\partial\mathbf{p}}\frac{d\mathbf{p}}{d\mathbf{b}}=-\frac{\partial\mathbf{F}_{\mathbf{int}}}{\partial\mathbf{b}}\ \text{ or }\ \mathbf{K}_t\frac{d\mathbf{p}}{d\mathbf{b}}=-\left(\frac{\partial\mathbf{F}_{\mathbf{int}}}{\partial\mathbf{b}}\right) \tag{20}$$

When computing the displacement derivatives, $\mathbf{K}_t$ is evaluated in the final state. The term on the right hand side of Eq. (20) requires computing the partial derivatives of the internal forces, $\partial\mathbf{F}_{int}/\partial\mathbf{b}$. Noting that displacements are obtained accurately using the iterative procedure within a load increment, the quasi-Eulerian approach is similar to the Eulerian approach wherein the net element internal forces can be expressed as

$$\mathbf{f}_{int}=\int_V\mathbf{B}_L^T\boldsymbol{\tau}dV \tag{21}$$

where $\mathbf{B}_L$ is the strain-displacement transformation matrix, $\boldsymbol{\tau}$ is the true or Cauchy stress vector, and V is the element volume. Partial differentiation of Eq. (21) with respect to design variables requires computing derivatives of $\mathbf{B}_L$, τ and V. $\mathbf{B}_L$, the strain-displacement transformation matrix is generally a constant with respect to the design variable in topology optimization. For geometrically nonlinear problems, $\boldsymbol{\tau}$ can be expressed as $\mathbf{C}\ \boldsymbol{\varepsilon}$ where $\mathbf{C}$ and $\boldsymbol{\varepsilon}$ are the constant constitutive material property tensor and Almansi strain tensor referred in the updated configuration. Explicit expressions for $\boldsymbol{\varepsilon}$ in terms of design variables are available for frame elements [15]. Partial differentiation of current volume V with respect to design can be ignored assuming that it is equal to the original volume for small strains.

The element internal force derivatives can be assembled in a similar manner as the internal forces in nonlinear solution procedure (Eq. 11). The force derivatives are assembled in a matrix of size $(n\times m)$ where n is the number of degrees of freedom and m is the number of design variables. Note that the inverse or factorized $\mathbf{K}_t$ is readily available from the analysis phase. Thus, solving Eqs. (20) involves additional back substitutions corresponding to the m vectors on the right hand side. In practice, for prescribed non-linear force-deflection characteristics, the displacement sensitivities for the entire load history are required. To avoid multiple analyses, this can be accomplished by simultaneously computing the sensitivities when calculating and accumulating the internal forces and thus their derivatives incrementally, as shown in Eq. (16).

Adjoint Variable Method

The efficiency in the direct differentiation approach can further be improved for known functions of displacements requiring sensitivity analysis, which usually is the case. Using the adjoint vari-

able method, for a function, ψ, an adjoint variable vector, $\boldsymbol{\mu}$ is introduced as follows [23]. Premultiplying Eq. (20) with $\boldsymbol{\mu}^{\mathbf{T}}$ and rearranging yields

$$[\mathbf{K}_t^T \boldsymbol{\mu}]^T \frac{d\mathbf{p}}{d\mathbf{b}} = -\boldsymbol{\mu}^{\mathbf{T}} \frac{\partial \mathbf{F}_{\mathbf{int}}}{\partial \mathbf{b}} \tag{22}$$

If μ is chosen to satisfy the equation

$$\mathbf{K}_t^T \boldsymbol{\mu} = \left(\frac{\partial \psi(\mathbf{b}^{\mathbf{c}}, \mathbf{p})}{\partial \mathbf{p}} \right)^{\mathbf{T}} \tag{23}$$

then the second term on the right hand side of Eq. (18) becomes

$$\frac{\partial \psi}{\partial \mathbf{p}} (\mathbf{b}^{\mathbf{c}}, \mathbf{p}) \frac{d\mathbf{p}}{d\mathbf{b}} = -\boldsymbol{\mu}^{\mathbf{T}} \frac{\partial \mathbf{F}_{\mathbf{int}}}{\partial \mathbf{b}} \tag{24}$$

To compare the two methods, the number of equations to be solved is considered. In the direct differentiation method, linear systems of equations with m vectors on the right hand side is solved while in the adjoint variable approach, linear systems constitute n_ψ such vectors. Here, n_ψ is the number of functions (objective and/or constraints) requiring sensitivity analysis. The adjoint variable method is more efficient when $m \gg n_\psi$. Nevertheless, the direct differentiation method can easily be modified to the adjoint variable approach given the displacement sensitivities of a prescribed degree of freedom (*pdof*) to be extracted. Premultiplying the right hand side of Eq. (20) by a vector L_{pdof} of size $1 \times n$, we get

$$\frac{d\mathbf{p}_{pdof}}{d\mathbf{b}} = -[\mathbf{L}_{pdof} \mathbf{K}_t^{-1}] \frac{\partial \mathbf{F}_{\mathbf{int}}}{\partial \mathbf{b}}; \quad [L_{pdof}]_j = 0$$

$$\text{if } j \neq pdof, \ 1 \quad \text{otherwise} \tag{25}$$

with the square parenthesis in Eq. (25) indicating the preference in multiplication. The operation within the parenthesis is equivalent to determining $\boldsymbol{\mu}^T$ in Eq. (24) using Eq. (23) [24].

The design sensitivities computed as described in Eq. (25) are compared and verified with the displacement inverter example shown in Fig. 5(*a*). The boundary conditions with input and output ports are shown in the figure. A force of 10 N is applied at the input port. The Young's Modulus is taken as 20 GPa and the out-of-plane width of the mechanism is 1 mm. The element in-plane thicknesses chosen as design variables are set to 1 mm. In the figure, solid lines represent the undeformed configuration while dotted lines show the deformed mechanism at different load increments. The frame element mesh with element numbers is shown in Fig. 5(*b*). Figure 5(*c*) compares the analytical design sensitivities of the output displacement with respect to the in plane widths of elements as design variables with those obtained from the finite difference method. The maximum error is less than 1%.

Synthesis Examples

The optimal topology solution procedure using two-dimensional geometrically nonlinear frame finite elements is first implemented for the synthesis of a micro displacement amplifier. In addition to deforming in the longitudinal direction, frame elements have the capability to deform in the transverse directions and therefore can incorporate bending modes. Consider the symmetric half of the meshed design domain of size 100 μm $\times$200 μm with input and output design requirements shown in Fig. 6(*a*). An input force, F_{in} of 500 μN is used as the actuation force. Polysilicon is used as the structural material with Young's Modulus of 169 GPa and the Poisson's ratio of 0.3. Respective in-plane thicknesses of the frame elements are chosen as design variables on which a lower bound of 10^{-3} μm and an upper bound of 4 μm are imposed. Variables reaching the lower bound are regarded as absent from the topology. The elements have a uniform out-of-plane width of 5 μm. For the amplifier design, the geometric advantage or the ratio of the output to input displacements is maximized. In standard form,

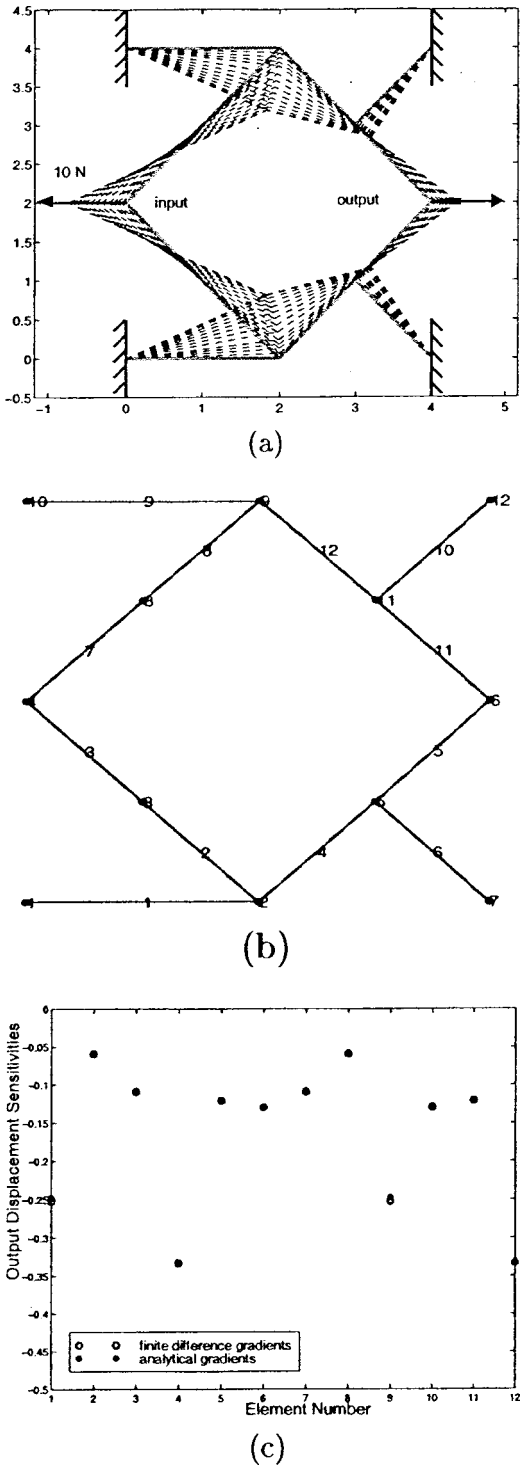

Fig. 5 Design sensitivity comparison with the displacement inverter example (*a*) input-output specifications (*b*) finite element mesh (*c*) comparison between analytical and finite difference sensitivities for the output displacement, maximum error =0.02%

$$\begin{aligned} &minimize: \ -\frac{\Delta_{out}}{\Delta_{in}} \\ &subject \ to: \ 10^{-3} \mu\text{m} \leqslant x_i \leqslant 4 \ \mu\text{m} \end{aligned} \tag{26}$$

To compute the function sensitivities, analytical derivatives of Δ_{out} and Δ_{in} are obtained using Eqs. (25). The optimization problem is solved using Sequential Quadratic Programming (SQP)

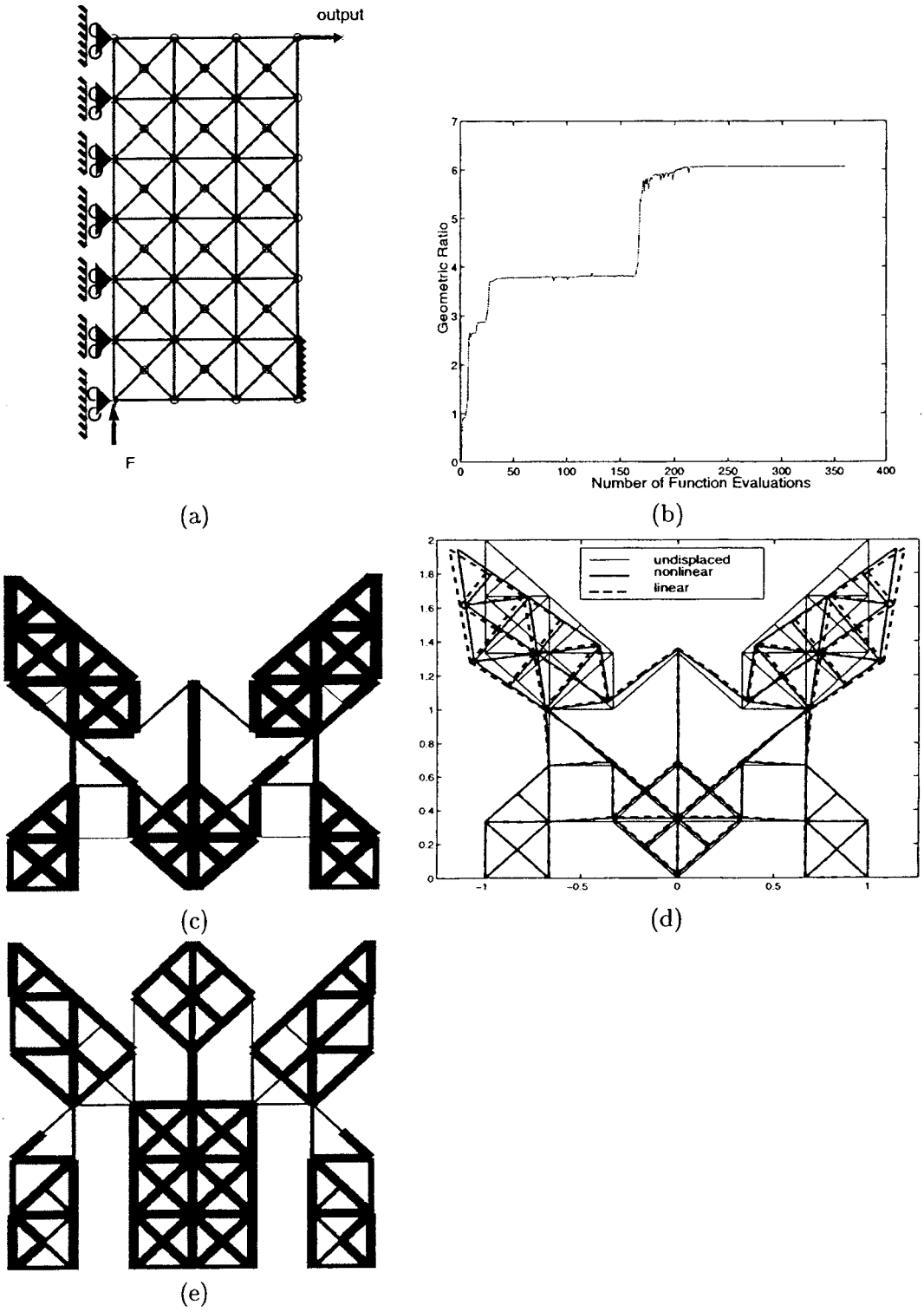

Fig. 6 Topological synthesis of a micro displacement amplifier. (*a*) Design specifications; $F=500\ \mu$N (*b*) convergence history for topology optimization (*c*) full section design of the displacement amplifier (*d*) displaced profile; geometric advantage is 6.2 (*e*) optimal topology for $F=100\ \mu$N.

technique in Matlab™ [17]. The convergence history for the optimization process is shown in Fig. 6(*b*). At convergence, the output deformation is 5.92 μm for which the geometric advantage (the objective function) is maximized to 6.2. The resultant full section topology of the displacement amplifier is shown in Fig. 6(*c*) with varying relative thicknesses of the elements. Figure 6(*d*) compares the results of linear and nonlinear analyses. Linear analysis yields an output deformation of 6.32 μm which is larger when compared with 5.92 μm obtained using nonlinear analysis. This is consistent with the phenomenon of geometric stiffening for structures undergoing large geometrically nonlinear deformation. Optimal topology is also obtained for the same design specifications but with an input load of 100 μN and is shown in Fig. 6(*e*). At convergence, the output displacement is 0.58 μm with the

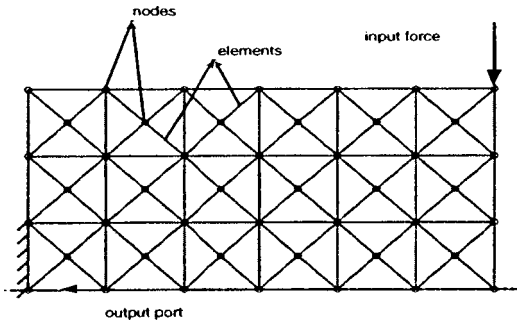

Fig. 7 Design domain for two-point compliant crimper force-deflection synthesis

geometric advantage of 2.89. The topology is slightly different when compared with Fig. 6(*c*) suggesting that optimal topologies may depend on the magnitude of the input load applied.

Linear analysis based synthesis is inaccurate in accounting for large deformations and proves inadequate in the design of compliant topologies for prespecified force-deflection characteristics as it assumes constant structural stiffness and therefore only linear deformation responses. With nonlinear analysis, quantitative accuracy along with the design framework for prespecified force-deflection characteristics can be obtained for compliant topologies undergoing large deformations. As an example, a monolithic crimper mechanism is designed for a *two-point* force-deflection specification. Figure 7 shows the symmetric half of the design domain with the input force and desired direction of motion of the output port. The domain is a 60 mm by 60 mm ground superstructure of geometrically nonlinear frame elements. The Young's modulus of the structural material is 2 GPa and the out-of-plane width of the mechanism is 1 mm. Respective in-plane thicknesses of the elements are chosen as design variables which are bound in the interval [0.001 mm, 3 mm].

One way of realizing the two-point force-deflection synthesis scheme is by minimizing the sum of the squares of the deformation residuals, that is

$$\begin{aligned} &\text{minimize} \quad \phi = \sum_{i=1}^{2} (\delta_i - \delta_i^*)^2 \\ &\text{subject to} \quad x_L \leqslant x_i \leqslant x_U \end{aligned} \tag{27}$$

where δ_i $(i=1,2)$ are the output deflection responses for input loads, F_i $(i=1,2)$ and δ_i^* $(i=1,2)$ are the respective desired output responses. The design variables, x_j, $(j=1,\ldots,N)$ are bounded within $[x_L, x_U]$ where x_L is a small positive quantity imposed to avoid singularity problems in the structural stiffness matrix. Elements for which the design variables assume the lower bound are regarded as absent from the continuum. To compute the function sensitivities, differentiating the objective in Eq. (27) gives

$$\frac{\partial \phi}{\partial x_j} = 2 \sum_{i=1}^{2} (\delta_i - \delta_i^*) \frac{\partial \delta_i}{\partial x_j}, \quad j=1,\ldots,N \tag{28}$$

The terms $\partial \delta_i / \partial x_j$ are the design sensitivities of the output deformations which can be obtained using Eq. (25). Optimal topologies

Table 1 Design specifications for the compliant crimper example

Case	F_1	F_2	δ_1^*	δ_2^*
I	10 N	20 N	2 mm	3 mm
II	10 N	20 N	2 mm	3.5 mm
III	10 N	20 N	2 mm	4.3 mm

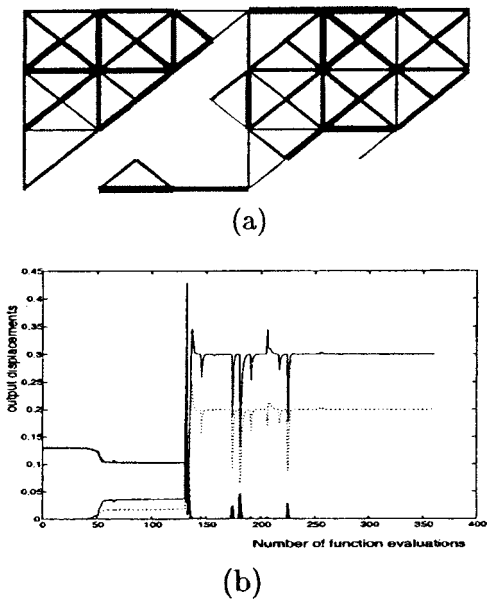

Fig. 8 Two-point force-deflection synthesis of a compliant crimper (*a*) optimal topology for design case I (*b*) convergence history

for the compliant crimpers are obtained for three specifications given in Table 1. Figure 8(*a*) shows the resultant topology for the design case I and the convergence history is shown in Fig. 8(*b*). The function shown using the thick solid line is minimized to zero in 350 function evaluations. The dotted line in the figure represents the output response for the load of 10 N and that shown in thin solid line represents the same for 20 N load. The optimal half section design for case II is shown in Fig. 9(*a*) with the convergence history in Fig. 9(*b*). The procedure requires about 250 function evaluations. Figures 10 depict the optimal design and history for case III. The force-deflection responses of the three designs are plotted in Fig. 11. Note that for each case, only one linear analysis is adequate and performed for the input load of 20 N. The

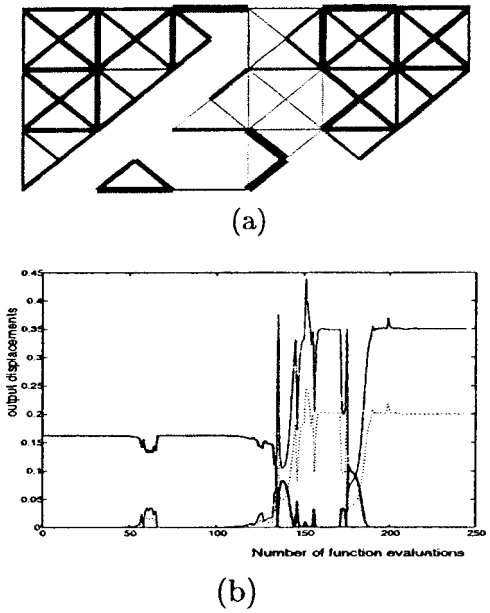

Fig. 9 Two-point force-deflection synthesis of a compliant crimper (*a*) optimal topology for design case II (*b*) convergence history

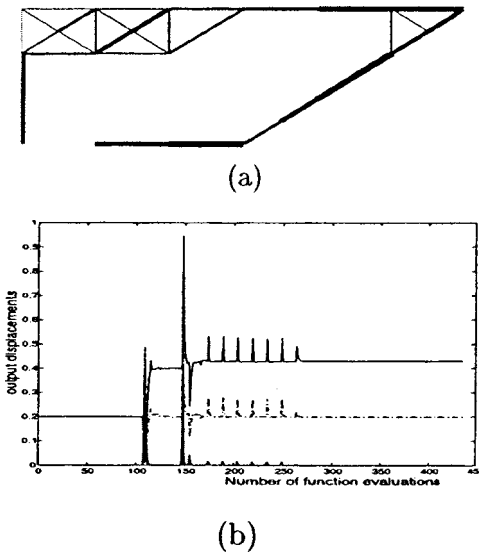

Fig. 10 Two-point force-deflection synthesis of a compliant crimper (*a*) optimal topology for design case III (*b*) convergence history

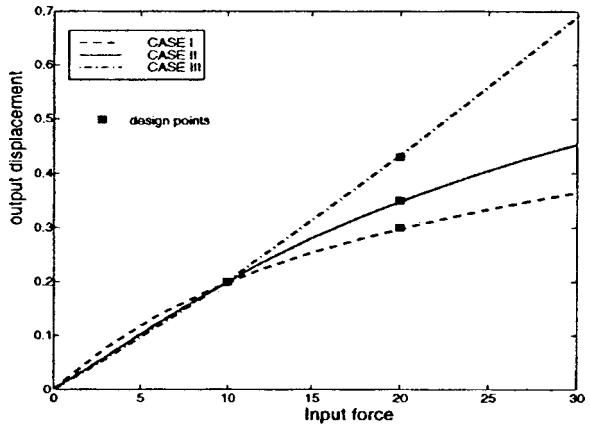

Fig. 11 Comparison of nonlinear force-deflection characteristics of the crimper designs (Figs. 8–10)

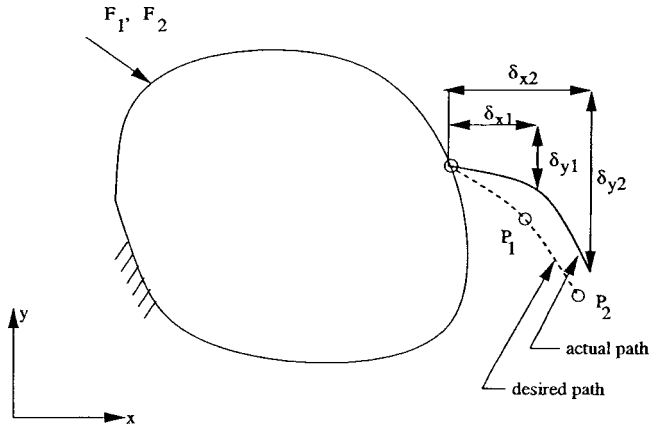

Fig. 12 Design specifications for prescribed curved output path

sensitivities at different time increments are stored and extracted/extrapolated for the required/intermediate time increments.

The two point force-deflection synthesis method can be extended to solve nonlinear topology synthesis problems involving curved output paths. For a given coordinate system, the output

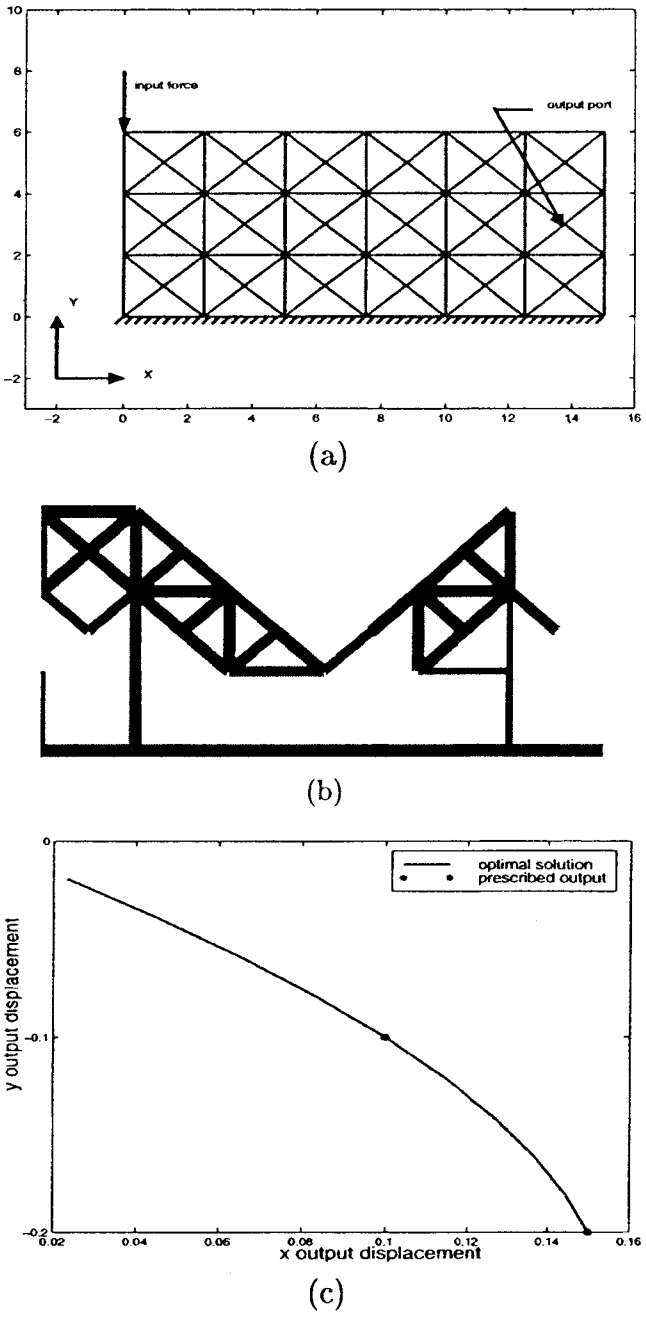

Fig. 13 (*a*) Design domain for compliant pliers (*b*) optimal pliers topology for specifications in Table 2 (*c*) output displacement trajectory for the optimal topology

port may need to traverse through points, P_1 and P_2 with coordinates, $(\delta x_1^*, \delta y_1^*)$ and $(\delta x_2^*, \delta y_2^*)$ with respect to its undeformed position as shown in Fig. 12. The two-point curved path synthesis method then requires the minimization the deformation residual. That is,

$$minimize: \quad \phi = \sum_{i=1}^{2} [(\delta x_i - \delta x_i^*)^2 + (\delta y_i - \delta y_i^*)^2] \qquad (29)$$

The formulation is similar to the three-precision point synthesis in kinematics literature. The output deformation sensitivities can be computed as described in previous sections. The first synthesis example is of a pliers mechanism. The design domain is shown in Fig. 13(*a*) which is a rectangular grid of 150 mm×60 mm with frame element discretization. Young's modulus of elements is as-

Table 2 Design specifications for the pliers example: Case I

Point	input force	δx^*	δy^*
P_1	10 N (vertically downward)	1 mm	− 1 mm
P_2	20 N (vertically downward)	2 mm	− 3 mm

Table 3 Design specifications for the pliers example: Case II

Point	input force	δx^*	δy^*
P_1	10 N (vertically downward)	1 mm	1.5 mm
P_2	20 N (vertically downward)	2 mm	2.5 mm

sumed as 2 GPa and out-of-plane widths are taken as 2 mm. In-plane thicknesses are the design variables which vary within the bounds [0.001 mm, 3 mm]. The curved output path specifications are given in Table 2. Since the initial optimization process is very slow for the objective in Eq. (29), topology synthesis is first performed with linear analysis using the flexibility-stiffness multicriteria formulation [9]. The output deformation is maximized along the tangent to the prescribed path at the undeformed position. The linear solution is taken as the initial guess for the subsequent nonlinear topology synthesis. Unfavorable elements causing instability, probably due to buckling, in objective and sensitivity evaluation are eliminated from the mesh periodically and the topology synthesis is resumed and continued until a final optimal topology is obtained. Size optimization is then performed with this topology with increased lower bound (1mm) to render the mechanism manufacturable. The optimal solution is shown in Fig. 13(*b*) and the deformation profile is depicted in Fig. 13(*c*). As can be seen from the figure, the prescribed curved path is traced precisely by the optimal topology in Fig. 13(*b*). For the same design domain, Young's modulus, element thicknesses and design variables as in the previous example, a reverse output path is

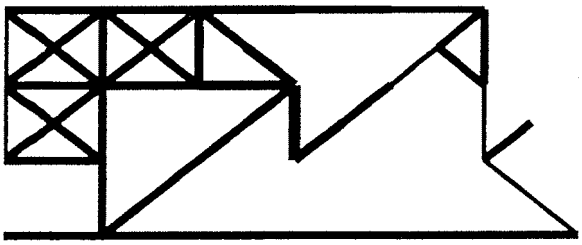

(a)

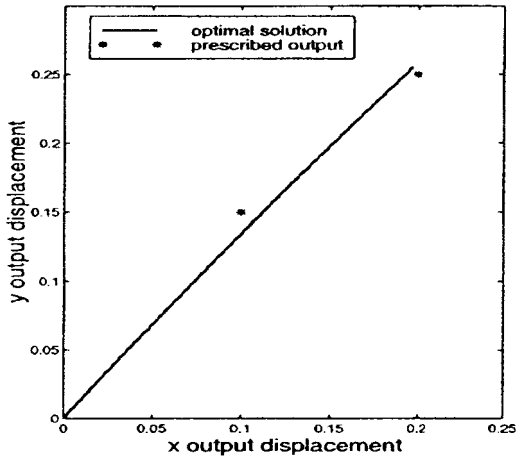

(b)

Fig. 14 (*a*) Optimal pliers topology for specifications in Table 3 (*b*) output displacement trajectory for the optimal topology

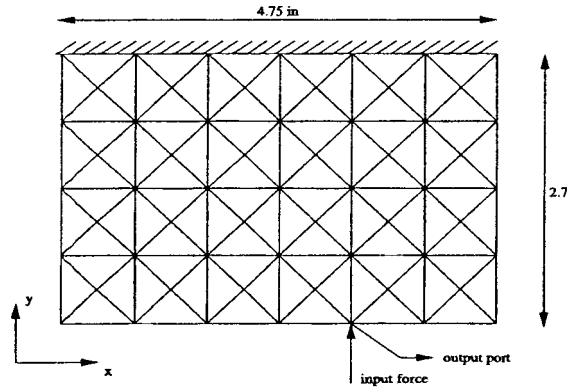

(a)

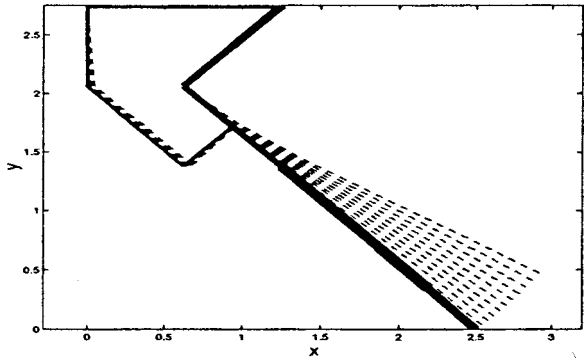

(b)

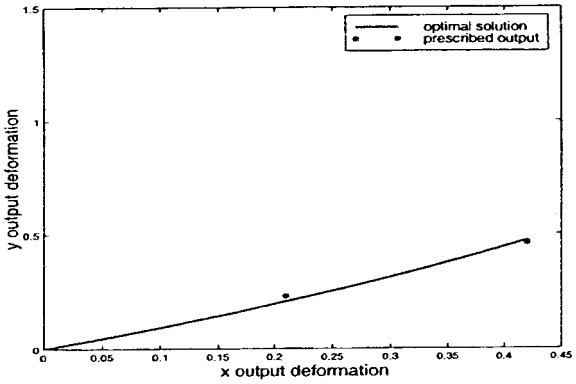

(c)

Fig. 15 (*a*) Design domain for the floppy drive loading mechanism (*b*) optimal topology (*c*) output displacement trajectory

attempted which is prescribed in Table 3. During size optimization, the lower and upper bounds were taken as 0.15 mm and 0.4 mm respectively. The optimal solution is shown in Fig. 14(*a*) and the output response is shown in Fig. 14(*b*). The error in the achieved and prescribed path is about 0.1%. Note that in solving force-deflection or path generation type problems, having springs at the output port to ensure force transmission is a design issue. A tendency of the designer to model output springs may exist to avoid the presence of thin elements near the output port. However, those springs should accurately model the interaction of the output port with the work piece over large displacement along a curved path. Inaccurate modeling or absence of springs, in such cases, might lead the output path to deviate from that prescribed.

Another example is the topology synthesis for the 3.5 in floppy drive loading mechanism [25] for prescribed linear output path. The design domain with loading and boundary conditions is shown in Fig. 15(*a*) and the prescribed output path is shown in

Table 4 Design specifications for the floppy drive example

Point	input force	δx^*	δy^*
P_1	2 N (vertically upward)	0.21 in	0.23 in
P_2	4 N (vertically upward)	0.42 in	0.46 in

Table 4. Here, two linear springs of constants 0.1 N/in are added along the x and y displacement directions at the output port to simulate the resistence along the linear path. As in the previous examples, topology synthesis is first performed using the linear finite element model. The optimal solution is then taken as the initial guess for the subsequent nonlinear synthesis. In case of non-convergence, the elements near their lower limit are removed and the synthesis process is resumed. Finally, size optimization is performed with the resultant topology with a lower limit of 1 mm. The final solution is shown in Fig. 15(b). Here, the solid lines represent undeformed configuration with relative element in-plane widths. The dotted lines represent the deformation for input load of 4 N in 10 load increments. Figure 15(c) compares the output deformation with that prescribed. As can be seen the prescribed path is nearly accurately traced by the output port with an error of about 0.2%.

Converting the optimal topologies to manufacturable form and exporting them into commercial CAD packages is relatively easy with frame elements. This is done using edge detection algorithms as described by Saxena et al. [6]. The resulting data is stored in the IGES format for easy portability into commercial modeling and analysis software packages.

Closure

Flexible members in compliant mechanisms undergo large deformations which cannot be modeled accurately using linear elastic elements in topology synthesis algorithms. Geometrically nonlinear finite element analysis is employed in this paper with frame elements to synthesize compliant mechanisms using the continuum based approach. A method for computing nonlinear design sensitivities that involves the direct differentiation of equilibrium equations with respect to the design variables is described. Nonlinear finite element model based optimization makes it possible to obtain quantitatively accurate solutions for compliant mechanisms with large deformations. Furthermore, their synthesis with prescribed nonlinear force-deflection characteristics and curved path for the output port is feasible as shown in this paper. Several synthesis examples are included to demonstrate the significance of nonlinear analysis procedures to design compliant mechanisms with accurate and controlled output behavior.

Acknowledgments

The authors would also like to acknowledge the Defense Advanced Research Projects Agency (DARPA) for financial support under the contract #537640-52247 and National Science Foundation (NSF) for CAREER award, DMI-9733916 (Ananthasuresh). The authors would also like to thank the anonymous reviewers for their useful suggestions.

References

[1] Howell, L., and Midha, A., 1996, ''A Loop-Closure Theory for the Analysis and Synthesis of Compliant Mechanisms,'' ASME J. Mech. Des., **118**, No. 1, pp. 121–125.
[2] Saxena, A., and Kramer, S. N., 1998, ''A Simple and Accurate Method for Determining Large Deflections in Compliant Mechanisms Subjected to End Forces and Moments,'' ASME J. Mech. Des., **120**, No. 3, pp. 392–400.
[3] Ananthasuresh, G. K., Kota, S., and Kikuchi, N., 1994, ''Strategies for Systematic Synthesis of Compliant MEMS,'' *Proc. of the 1994 ASME Winter Annual Meeting*, Nov. 1994, Chicago, IL, pp. 677–686.
[4] Frecker, M. I., Ananthasuresh, G. K., Nishiwaki, N., Kikuchi, N., and Kota, S., 1997, ''Topological Synthesis of Compliant Mechanisms using Multi-Criteria Optimization,'' ASME J. Mech. Des., **119** pp. 238–245.
[5] Sigmund, O., 1997, ''On the Design of Compliant Mechanisms Using Topology Optimization,'' Mech. Struct. Mach., **25**, No. 4, pp. 495–526.
[6] Saxena, A., Wang, X., and Ananthasuresh, G. K., 2000, ''PennSyn: A Topology Synthesis Software for Compliant Mechanisms DETC/MECH-14139,'' *ASME Design Engineering Technical Conferences*, September, 10–13, Baltimore, MD.
[7] Nishiwaki, S., Frecker, M. I., Min, S., and Kikuchi, N., 1998, ''Topology Optimization of Compliant Mechanisms using the Homogenization Method,'' Int. J. Numer. Methods Eng., **42**, pp. 535–559.
[8] Saxena, A., and Ananthasuresh, G. K., 1998, ''An Optimality Criteria Approach for the Topology Synthesis of Compliant Mechanisms-DETC/'99 DAC,'' *Proceedings of the DETC'98, ASME Design, Engineering Technical Conference*, Sept. 13–16, Atlanta, Georgia, DETC98/MECH-5937.
[9] Saxena, A., and Ananthasuresh, G. K., 2000, ''On an Optimal Property of Compliant Mechanisms,'' Struct. Multidisciplinary Optim., **19**, No. 1, pp. 36–49.
[10] Larsen, V. D., Sigmund, O., and Bouwstra, S., 1996, ''Design and Fabrication of Compliant Mechanisms and Structures with Negative Poisson's Ratio,'' *IEEE, International Workshop on Micro Electro Mechanical Systems*, MEMS-96.
[11] Hetrick, J. A., and Kota, S., 1999, ''An Energy Formulation for Parametric Size and Shape Optimization of Compliant Mechanisms,'' ASME J. Mech. Des., **121**, No. 2, pp. 229–234.
[12] Bruns, T. E., and Tortorelli, D. A., 1998, ''Topology Optimization of Geometrically Nonlinear Structures and Compliant Mechanisms,'' *Proc. of the 7th AIAA/USAF/NASA/ISSMO Symposium on Multidisciplinary Analysis and Optimization*, AIAA-98-4950, pp. 1874–1882.
[13] Buhl, T., Claus, B., Pedersen, W., and Sigmund, O., 1999, ''Stiffness Design of Geometrically Nonlinear Structures using Topology Optimization,'' DCAMM Report No 614, Danish Center for Applied Mathematics and Mechanics, Apr. 1999.
[14] Pedersen, C., Buhl, T., and Sigmund, O., 1999, ''Topology Synthesis of Large Displacement Compliant Mechanisms,'' *Proceedings of 1999 ASME-DETC*, Las Vegas, September, DETC99/DAC-8554.
[15] Crisfield, M. A., 1991, *Nonlinear Finite Element Analysis of Solids and Structures*, Vol. 1, John Wiley & Sons Limited, Baffins Lane, Chichester, PO19 1UD, England.
[16] Bathe, K. J., 1996, *Finite Element Procedures*, Prentice Hall, Englewood Cliffs, New Jersey 07632.
[17] Matlab™, 2000, *The Language of Technical Computing, Student Edition*, 5th Ed., The MathWorks Inc., 24 Prime Park Way, Natick, MA, 01760-1500.
[18] ABAQUS™, 1996, *Abaqus/Standard User's Manual*, Hibbit, Karlsson & Sorensen, Inc. 1080 Main Street, Pawtucket, RI 02860-4847, Ver. 5.6.
[19] Santos, J. L. T., and Choi, K. K., 1992, ''Shape Design Sensitivity Analysis of Nonlinear Structural Systems,'' Struct. Optim., **4**, pp. 23–35.
[20] Choi, K. K., and Huag, E. J., 1983, ''Shape Design Sensitivity Analysis of Elastic Structures,'' J. Struct. Mech., **11**, pp. 231–269.
[21] Choi, K. K., and Santos, J. L. T., 1987, ''Design Sensitivity Analysis of Nonlinear Structural Systems, Part I: Theory,'' Int. J. Numer. Methods Eng., **24**, pp. 2039–2055.
[22] Santos, J. L. T., and Choi, K. K., 1988, ''Sizing Design Sensitivity Analysis of Nonlinear Structural Systems. Part II: Numerical Method,'' Int. J. Numer. Methods Eng., **26**, pp. 2097–2114.
[23] Ryu, Y. S., Haririan, M., Wu, C. C., and Arora, J. S., 1985, ''Structural Design Sensitivity Analysis of Nonlinear Response,'' Comput. Struct., **21**, pp. 245–255.
[24] Claus, B., Pedersen, W., Buhl, T., and Sigmund, O., 2000, ''Topology Synthesis of Large Displacement Compliant Mechanisms,'' DCAMM Report No 631, Danish Center for Applied Mathematics and Mechanics, Jan. 2000.
[25] Yahya, R., 1999, ''One Piece Compliant Disk-Drive Loading Mechanism,'' Capstone design project report, Mechanical Engineering and Applied Mechanics, University of Pennsylvania, Philadelphia, PA.